

Appendix C

Finite Element Modeling

C.1 Material Models

To achieve the goal of the 3D FEM study, realistic material models capturing the mechanical responses of the constituent materials and behaviors are essential. In a girder containing partially debonded prestressing strands, the primary constituents are concrete, prestressing steel, and the bond behavior at the concrete-strand interface. The material library of ATENA contains a variety of advanced constitutive models, which are capable of capturing concrete behaviors under bi- and tri-axial loading, nonlinear performance of the concrete-steel interface, and concrete cracking in disturbed regions (so called D-regions). In addition, it may be easily used to reproduce complex construction sequences. ATENA is able to realistically approximate the response of RC members at each construction step and at each load level, which, for this project, is an important advantage over other FEM software.

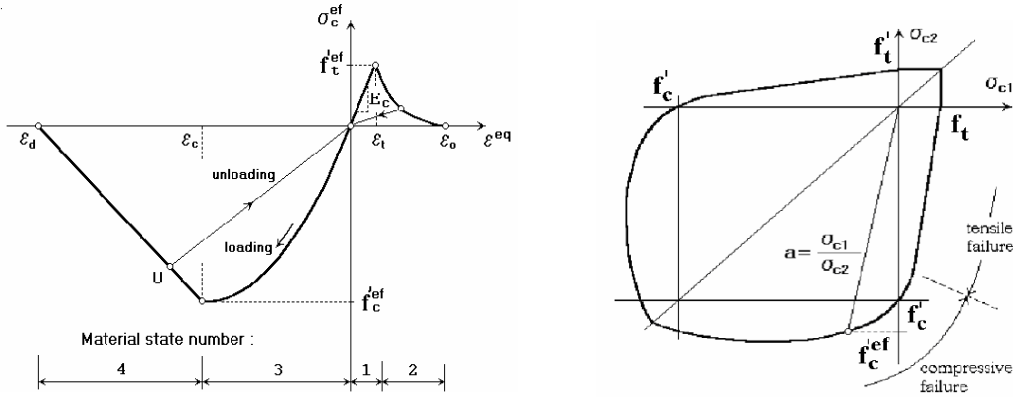
C.1.1 Material Model for Concrete

A fracture-plastic model is employed to describe the behavior of concrete. The model, consisting of a fracture model based on a smeared crack formulation and crack band concept and a plasticity model residing on a plastic failure surface, is intended to accurately capture concrete behavior in tension (fracture) and compression (crushing). The smeared crack formulation and crack band concept is widely used in fracture mechanics to ensure that the stress-strain calculation is consistent with the required continuum mechanics. A discrete crack in an element is treated as an equivalent cracking strain, which is uniformly distributed across the whole element. However, the size of the element cannot be arbitrary. It must satisfy the physical requirement of micro-crack localization and fracture energy dissipation. This element size of physical significance is called the crack band. An important advantage of the smeared crack formulation and crack band concept is that an *a priori* crack path is not needed in modeling.

The equivalent uniaxial stress-strain model for concrete implemented in the ATENA model is shown in Figure C.1a in which, phases 1, 2, 3 and 4 shown on the horizontal axis represent the loading and softening in tension and compression. The biaxial stress failure envelope, which is similar to the criterion proposed by Kupfer et al. (1969), is shown in Figure C.1b. In the fracture model, an exponential softening is assumed for concrete after it reaches its tensile strength. For the plasticity model, a hardening/softening failure surface is followed. When combining these two models, the following important interactions are taken into account:

1. Tensile strength reduction after concrete crushing, which is captured by adding equivalent plastic strain to tensile damage;
2. Compressive strength reduction after concrete cracking, which is described using the modified compression field theory (Vecchio and Collins 1986);
3. Shear strength of cracked concrete, which is calculated based on the modified compression field theory (Vecchio and Collins 1986).

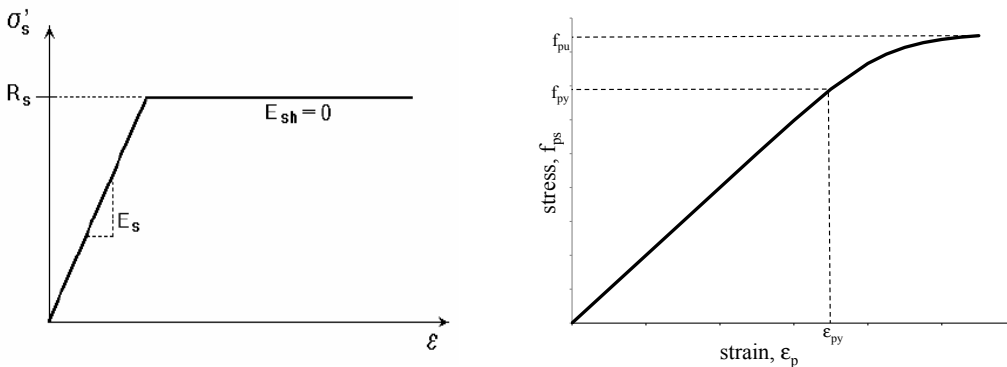
Unlike plain concrete, in reinforced or prestressed concrete, cracks cannot be fully developed to eliminate the concrete contribution to the steel stiffness. This effect is referred as tension stiffening and is considered in the constitutive model used based on the CEB-FIP model (1990). The fracture-plastic model for concrete contains a number of free material and mechanical parameters, some of which are allowed to vary so as to capture the behaviors of concrete under different stress conditions. In the present study, default values or values based on AASHTO-prescribed formulas are assigned to these parameters. The only free parameter in the modeling conducted is the compressive strength of concrete.



(a) Uniaxial stress-strain relation (b) Biaxial failure surface
Figure C.1. Constitutive model for concrete (ATENA)

C.1.2 Material Model for Prestressing Strands and Normal Reinforcement

For non-prestressed reinforcement, the classical elasto-plastic material model is employed. The stress-strain relationship is characterized by the bilinear constitutive law shown in Figure C.2a. The initial ascending part of the bilinear law is governed by the Young's modulus of steel, E_s , and the horizontal plateau is dictated by the yield strength and limit strain. For prestressing strands, a more accurate representation of the strand response, based on a Ramberg-Osgood model, is used to describe the nonlinear stress-strain relation. The "yield stress", f_{py} , is specified at a strain of $\epsilon_{py} = 1\%$, as shown in Figure C.2b.



(a) Bilinear stress-strain law for non prestressed reinforcement (b) Ramberg-Osgood model for prestressing strands

Figure C.2. Constitutive models for steel

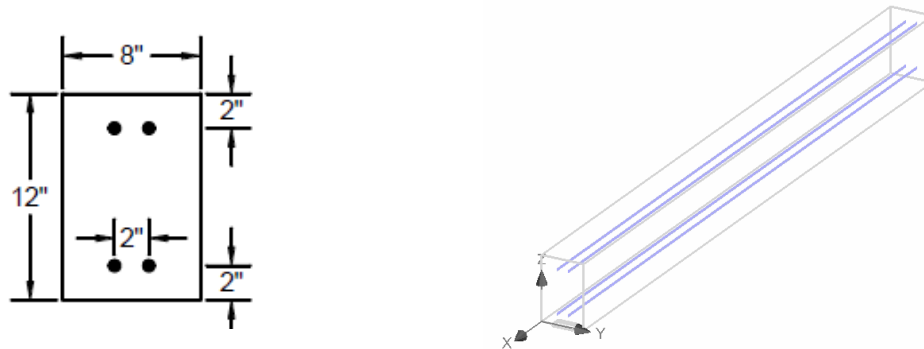
C.1.3 Model for Concrete-Strand Interface

For all non-prestressed reinforcement such as stirrups and slab reinforcement, a rigid connection is assumed between concrete and reinforcement. Thus, a perfect bond without any slips results. The rationale for selecting a perfect bond for non-prestressed reinforcement is that sufficient anchorage is provided in all cases.

For the prestressing strands, perfect bond with the surrounding concrete is not realistic. In fact, bond slip can initiate immediately upon prestress transfer. In the present study, a bond model following the formulation of the CEB-FIP model (1990) is used to describe the mechanical interaction at the concrete-strand interface. In this model, a nonlinear bond-slip relationship is characterized by a multi-linear constitutive law. Softening will occur if the slip exceeds a certain

limit. The key parameters in the constitutive law are the maximum bond strength, plastic limit, linear softening limit and residual bond strength. The values of these parameters depend on the concrete strength, reinforcement type and confinement condition (which can be adjusted to also capture the Hoyer effect based on the initial prestress level in the strand). In this study, the values of the governing parameters used in the bond model are selected such that they result in a prescribed value of transfer length equal to 30 or 60 strand diameters (d_b).

In the 3D FEM study, the bond-slip models resulting in different transfer lengths: $30d_b$ (“realistic”), $60d_b$ (AASHTO-prescribed) of three strand diameters: 0.5 in., 0.6 in., and 0.7 in. are calibrated using the simple experimental investigation reported by Burgueno and Yi (2011). In their tests, pre-tensioned beams were manufactured and the stress development in the strands was evaluated based on data from strain gauges. The R4 girder in their tests is selected to calibrate the bond-slip model. The 20-foot long girder R4 has a rectangular cross section 12 in. by 8 in. and is reinforced with four 0.6 in. 270 ksi low-relaxation prestressing strands as shown in Figure C.3. The compressive strength and modulus of concrete was 7.37 ksi and 4894 ksi, respectively, at prestress transfer.



(a) girder cross section of R4 girder

(b) Girder FEM model

Figure C.3. Geometry of 20-foot long girder R4 (Burgueno and Yi 2011)

ATENA generates a multi-linear bond-slip constitutive model following the formulation of CEB-FIP model (1990). This model is based on the concrete strength, reinforcement type and confinement condition given and is shown as the “prototype” model in Figure C.4. The model was first calibrated using the results reported by Burgueno and Yi. In the FEM of the Burgueno and Yi beam R4, the size of steel element is about 200 mm, which is sufficient to avoid spurious energy dissipation caused by coarse meshing. A mesh sensitivity analysis showed that reducing the element size to 100 mm or enlarging it to 500 mm did not significantly affect modeled behavior as shown in Figure C.5. Using the calibrated model, stress slip relationships are found for 0.5 in., 0.6 in. and 0.7 in. strands that result in the prescribed transfer lengths (i.e., $30d_b$ or $60d_b$).

In the Burgueno and Yi tests, the ultimate strength of all strands is 270 ksi, and the measured transfer length was about 26 in. ($43d_b$). The bond-slip models for different strand diameters and target transfer lengths are obtained by scaling the prototype bond-slip model. For instance, the scale factor required to achieve the AASHTO-prescribed transfer length of $60d_b$ is 2.60 as shown in Figure C.4.

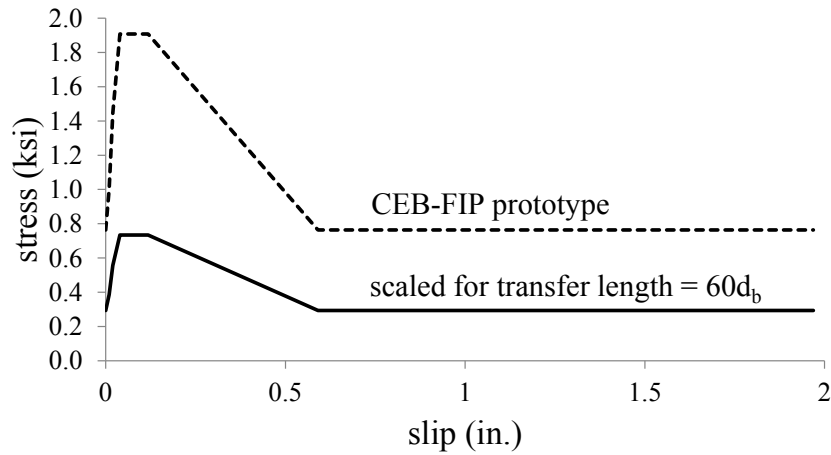


Figure C.4. Bond slip models for 3D FEM

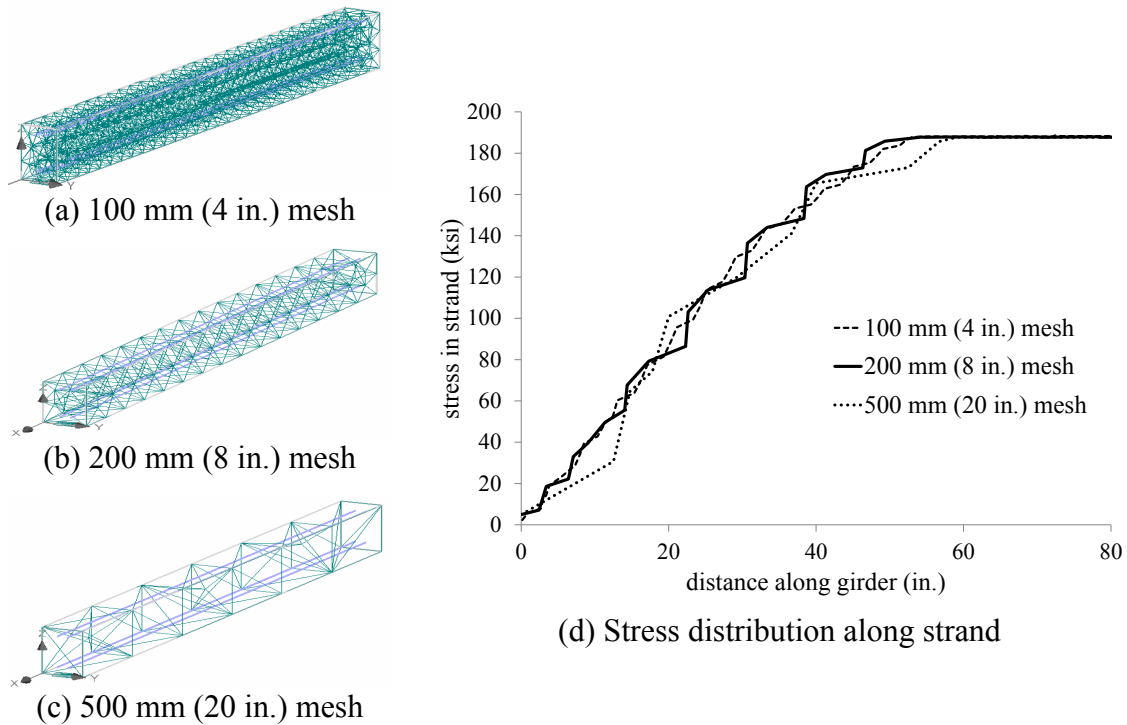


Figure C.5. Mesh sensitivity analysis for the bond-slip model used in simulation

C.2 Structural Modeling

The aforementioned material models are all found in the ATENA material library. In addition to the material models, ATENA also provides the tools required to simulate the construction and loading process of the prestressed girders. In the modeling, the prestressed girder is represented as a 3D model. The concrete of the girder is meshed with 3D hexahedral elements, while the reinforcement and prestressing strands are modeled with 3D truss elements. Their interaction is captured by the bond-slip model described above based on the relative displacement between the steel truss element and the surrounding hexahedral concrete element.

In the modeling, the prestress of the strands is modeled in a manner similar to the practice of prestressing. A force required to generate the desired prestress, is applied to the strand. After

concrete is “cast” (concrete modeled with properties corresponding to those at prestress transfer), the external force is deactivated to simulate the prestress transfer. The construction of the slab is modeled similarly. Initially, the top slab is “deactivated” during girder construction, so that it has no effect at prestress transfer. Following this, and an increase in the underlying girder concrete strength, the top slab load is first applied and then the slab is “activated” to work together with the girder to resist the simulated AASHTO-prescribed STRENGTH I and SERVICE I and III loading. In this manner, the critical loading stages for the prestressed girder are modeled in a realistic manner.

In addition to output files, ATENA provides a post-processing interface to graphically illustrate the simulation results. The stress and strain in concrete and strands can be graphically demonstrated on the model, as well as the cracks shown. Based on the crack band model used in the material model for concrete, damage in the concrete after reaching its tensile strength is characterized by an exponential softening. When the softening reaches a critical strain, cracking (visible separation of material) occurs. ATENA permits a threshold level of damage to be illustrated; that is: only damage (crack widths) greater than this threshold are shown in output graphics.

C.3 Validation of FEM Model

Two FEM models of previous laboratory-tested girders are used to validate the FEM model. NCHRP Report 579 (Hawkins and Kuchma 2007) reports twenty experiments of ten 63 in. deep and 52 ft long bulb-tee girders. The geometry of the test girders is shown in Figure C.6. Each simply supported member was designed to span 50 ft and to carry a uniformly distributed load over the central 44 ft of its length. A 10 in. deep composite slab was cast on each girder extending only the 42 in. width of the top flange (Figure C.6a). Each half of each girder (designated East [E] and West [W]; see Figure C.6b) was designed to be different so as to obtain two test results from each girder.

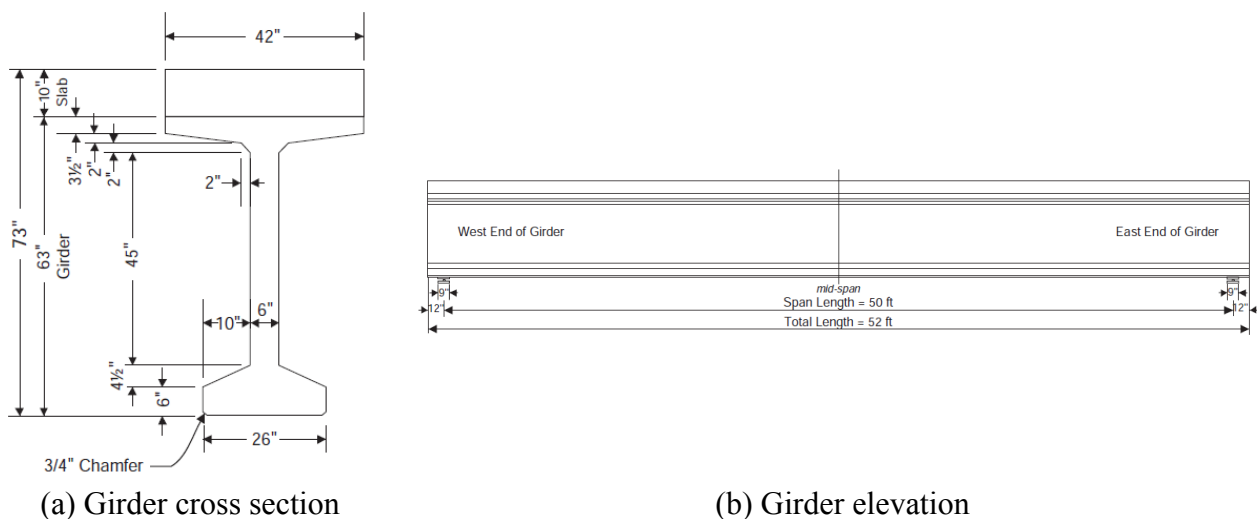


Figure C.6. Geometry of 63 in. bulb tee girders with slabs (Hawkins and Kuchma 2007)

Two girders – Girder 1 and Girder 6 – were selected for the validation study. Girder 1 is reported in detail in NCHRP Report 579 while similar reporting of Girder 6 is contained in the Appendices of the same report. The details of each girder are reported in Table C.1 and as follows.

Girder 1, shown in Figure C.7a, had 32 – 0.6 in. diameter strands in the bulb and two strands in the top flange. In the East end (1E) all were straight, while 6 strands were harped in the West end (1W). There was no strand debonding provided. Primary shear reinforcement consisted of No. 4 stirrups at 12 in.

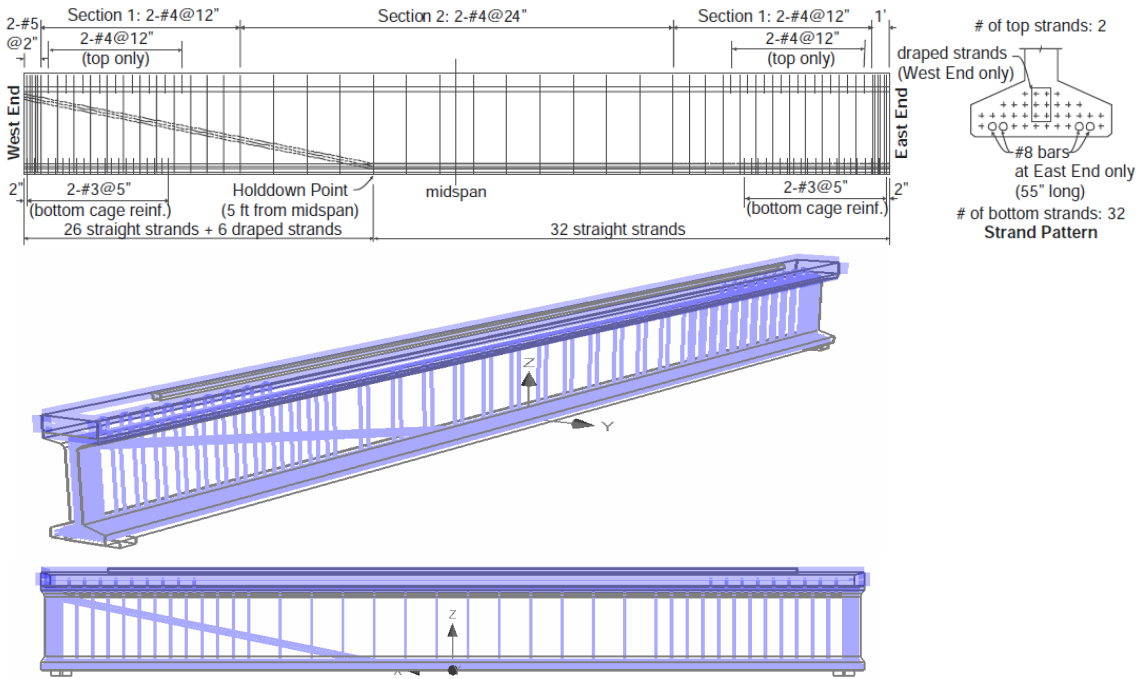
Girder 6, shown in Figure C.7b, had 42 – 0.6 in. diameter straight strands in the bulb and two strands in the top flange. At the West end (6W), 16 of the bottom strands and both top strands were partially debonded over lengths varying from 2 to 10 ft (Figure C.7b). In the East end (6E) all strands were fully bonded. Primary shear reinforcement consisted of No. 5 stirrups at 12 in.

All material properties used in the FEM are consistent with those reported by Hawkins and Kuchma and are reported in Table C.1 and were implemented as described previously.

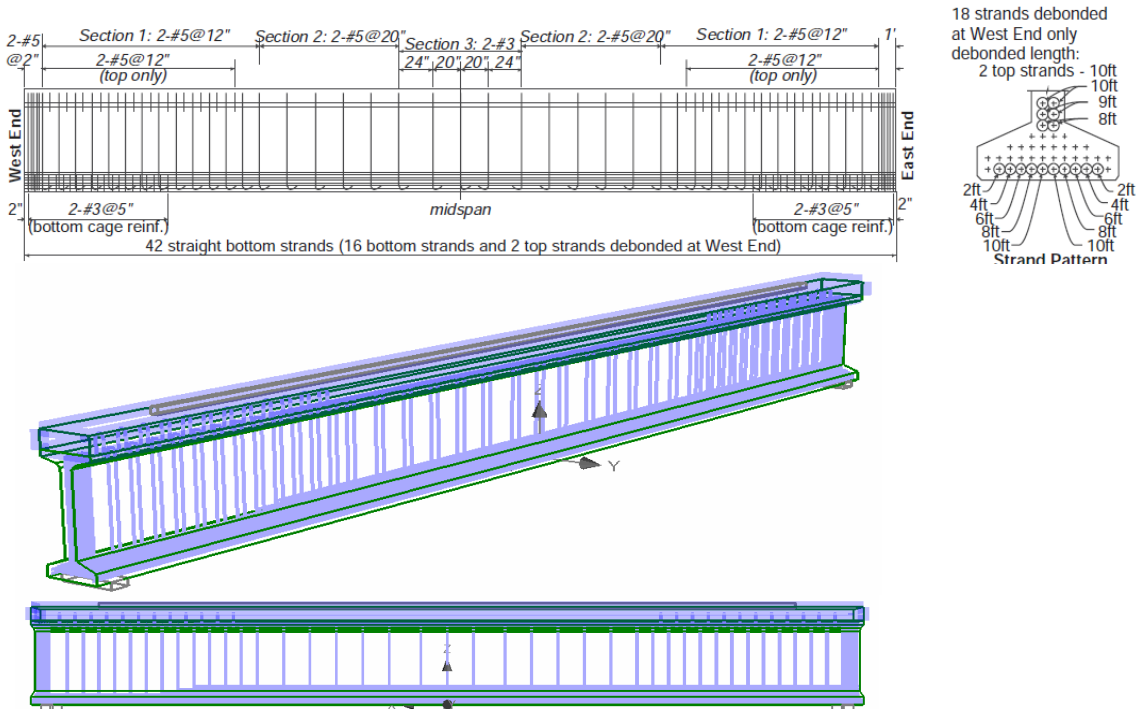
Based on elastic shortening measurements reported by Hawkins and Kuchma, the actual transfer lengths were determined to range from 18 to 28 in., with an average of about 23 in., about two-thirds of the AASHTO LRFD-prescribed value of $60d_b = 36$ in. In order to capture the real transfer lengths observed in the experiments, the bond-slip model described previously was scaled to match the experimentally-reported transfer lengths.

Table C.1. Experimental girder geometry and material properties

	Girder 1		Girder 6	
	1E	1W	6E	6W
Detail				
0.6 in. bottom strands	32 straight	26 straight 6 harped	42 straight	42 straight 18 debonded
0.6 in. top strands	2 straight		2 straight	2 straight 2 debonded
Section 1 stirrups (Fig. C.7)	No. 4 @ 12 in.		No. 5 @ 12 in.	
Section 2 stirrups (Fig. C.7)	No. 4 @ 24 in.		No. 5 @ 20 in.	
Section 3 stirrups (Fig. C.7)	-		No. 3 @ 24 in.	
Concrete Properties				
Compressive strength	12.1 ksi		12.7 ksi	
Strain at compression strength	3000 $\mu\epsilon$		2800 $\mu\epsilon$	
Split tensile strength	867 psi		823 psi	
Modulus of rupture	991 psi		1190 psi	
Deck compressive strength	4.5 ksi		9.2 ksi	
Strand Properties				
Ultimate capacity	$f_{pu} = 270$ ksi		$f_{pu} = 270$ ksi	
Initial prestress	202.5 ksi = 0.75 f_{pu}		202.5 ksi = 0.75 f_{pu}	
Prestress loss	21.1%		17.2%	
Effective stress	159.7 ksi		167.6 ksi	
Measured transfer length	28 in.	28 in.	23 in.	n.a.
Reinforcing Steel Properties				
Bar size	No. 4		No. 5	
Yield strength	70.0 ksi		64.7 ksi	
Ultimate strength	109.0 ksi		102.0 ksi	



(a) Girder 1 details (Hawkins and Kuchma 2007) and FEM model



(b) Girder 6 details (Hawkins and Kuchma 2007) and FEM model

Figure C.7. Experimental girders reported by Hawkins and Kuchma (2007)

In order to validate the 3D FEM model, the experimental girders 1 and 6 were modeled using ATENA in a manner identical to that adopted for the analytical study. Oblique and elevation views of the validation models are shown in Figure C.7. In order to accurately capture the girder construction process, the analysis is divided into four loading phases: (1) casting girder (step 1); (2) prestressing strand release (steps 2-7); (3) cast top slabs (step 8); and (4) external loading as described in Hawkins and Kuchma (steps 9-26).

In the experiment, Girder 1 failed at the East end (without harping), at an applied uniform load (applied over the middle 44 feet of the girder length) of 26.03 kip/ft. The FEM simulation predicts the same failure at 26.0 kip/ft. In the experiments, Girder 6 failed at the West end (having partial debonding), at an applied load ranging from 27.85 to 30.0 kip/ft. The FEM simulation predicts the same failure at 27.5 to 28.5 kip/ft. Both results indicate excellent agreement between the FEM-predicted and experimental behavior.

Crack patterns and load displacement behavior are used to validate the FEM results. Tables C.2 and C.3 summarize observed and FEM-predicted crack patterns for Girders 1 and 6, respectively. The “crack threshold” used to plot the crack patterns from the FEM was 0.0079 in. (0.2 mm); for clarity, no crack smaller than this is shown. In general, predicted crack patterns match well with experimental results. In particular, the splitting failure associated with partial debonding of Girder 6 is captured by the FEM model.

Experimental and predicted vertical deflections at four points along the span (midspan and approximate quarter points; labeled V1 through V5 in Figure C.8) are compared in Figure C.8, again showing excellent agreement. In Figure C.8, the FEM-predicted load-deflection plots (dotted lines) are overlaid directly on those reported by Hawkins and Kuchma. The FEM model is unable to capture behavior beyond the first failure (West end) of Girder 6; in the experimental study, the West end was repaired and testing continued until East end failure (shown in Figure C.8b).

Based on the ability to accurately model the detailed behavior of Hawkins and Kuchma girders 1 and 6, the 3D FEM model, implemented in ATENA is appropriately validated.

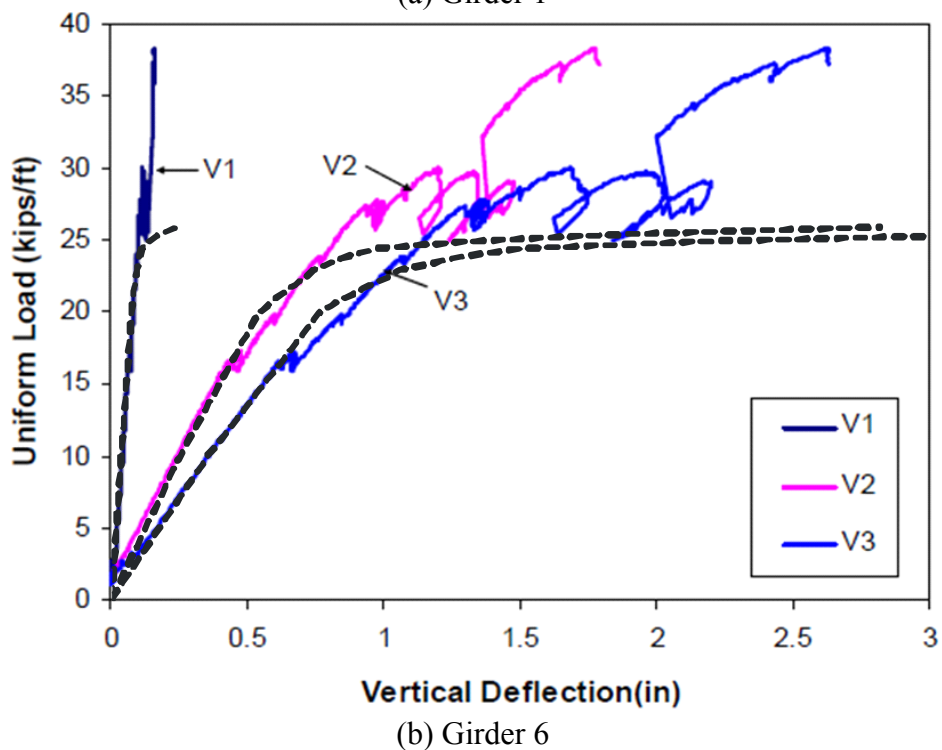
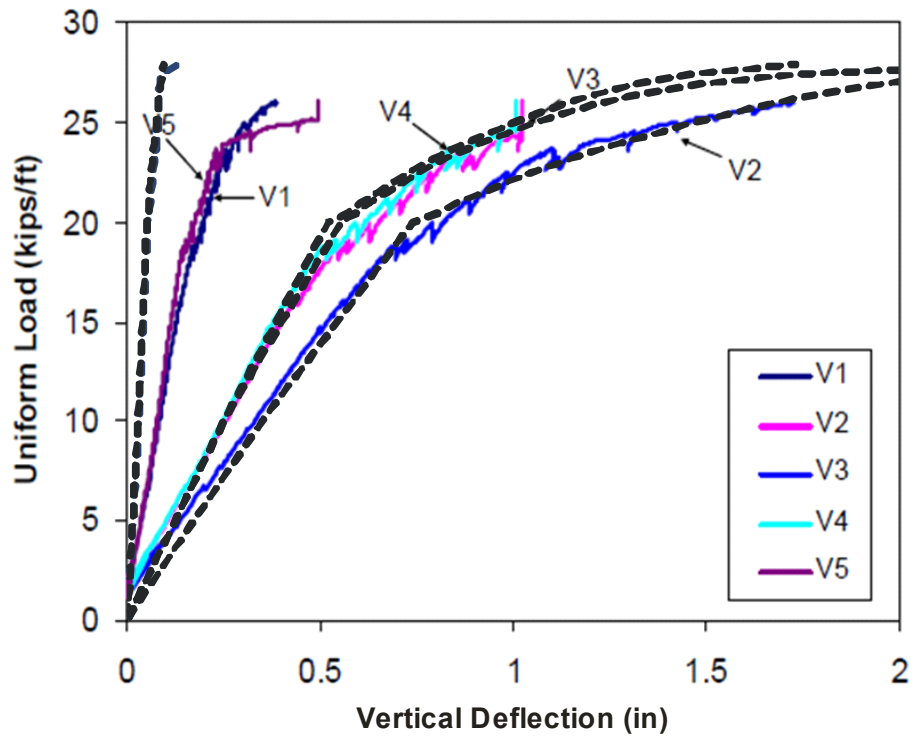


Figure C.8. FEM-predicted load-deflection curves (dotted) overlaid on those reported by Hawkins and Kuchma (2007)